

On Iron Monoxide Nanoparticles as a Carrier of the Mysterious $21\ \mu\text{m}$ Emission Feature in Post-Asymptotic Giant Branch Stars

Aigen Li¹, J.M. Liu², and B.W. Jiang^{2,1}

ABSTRACT

A prominent, mysterious emission feature peaking at $\sim 20.1\ \mu\text{m}$ — historically known as the “ $21\ \mu\text{m}$ ” feature — is seen in over two dozen Galactic and Magellanic Cloud carbon-rich post-asymptotic giant branch (post-AGB) stars. The nature of its carrier remains unknown since the first detection of the $21\ \mu\text{m}$ feature in 1989. Over a dozen materials have been suggested as possible carrier candidates. However, none of them has been accepted: they either require too much material (compared to what is available in the circumstellar shells around these post-AGB stars), or exhibit additional emission features which are not seen in these $21\ \mu\text{m}$ sources. Recently, iron monoxide (FeO) nanoparticles seem to be a promising carrier candidate as Fe is an abundant element and FeO emits exclusively at $\sim 21\ \mu\text{m}$. In this work, using the proto-typical protoplanetary nebula HD 56126 as a test case, we examine FeO nanoparticles as a carrier for the $21\ \mu\text{m}$ feature by modeling their infrared emission, with FeO being stochastically heated by single stellar photons. We find that FeO emits too broad a $21\ \mu\text{m}$ feature to explain the observed one and the Fe abundance required to be locked up in FeO exceeds what is available in HD 56126. We therefore conclude that FeO nanoparticles are unlikely responsible for the $21\ \mu\text{m}$ feature.

Subject headings: circumstellar matter — dust, extinction — infrared: stars — stars: AGB and Post-AGB — stars: individual (HD 56126)

1. Introduction

During the late stages of evolution, low- and intermediate-mass ($0.8 M_{\odot} < M < 8 M_{\odot}$) stars undergo a rapid transition phase of several thousand years between the asymptotic giant branch (AGB) phase and the planetary nebula (PN) phase. Objects in this short-lived stage of evolution are known as protoplanetary nebulae (PPNe), a term which is often used interchangeably with “post-AGB stars”.

¹Department of Physics and Astronomy, University of Missouri, Columbia, MO 65211, USA; lia@missouri.edu

²Department of Astronomy, Beijing Normal University, Beijing 100875, China; bjiang@bnu.edu.cn

Dust is a general phenomenon of PPNe, as revealed by its thermal infrared (IR) emission continuum and spectral features. In recent years, much attention has been paid to the so-called “21 μm feature”. This prominent, broad, mysterious emission feature, with a peak wavelength at $\sim 20.1 \mu\text{m}$ and a FWHM of $\sim 2.2\text{--}2.3 \mu\text{m}$, was first detected in four PPNe (Kwok et al. 1989). To date, it has been seen in 18 Galactic objects (Cerrigone et al. 2011) and 9 Magellanic Cloud objects (Volk et al. 2011), all of which are exclusively PPNe. The 21 μm feature exhibits little shape variation among different sources. The 21 μm sources exhibit quite uniform characteristics: they are metal-poor, carbon-rich F and G supergiants with strong IR excess and over abundant s-process elements (see Jiang et al. 2010).

The carrier of the 21 μm feature remains unidentified, although over a dozen candidate materials have been proposed. Zhang et al. (2009a) examined nine inorganic carrier candidates for the 21 μm feature, including nano TiC, fullerenes with Ti, SiS₂, doped SiC, silicon and carbon mixture, SiO₂-coated SiC, and iron oxides (FeO, Fe₂O₃ and Fe₃O₄). They found that except FeO nanoparticles, they are all problematic: they either require too much dust material (compared to what would be available in the 21 μm sources) or produce extra features which are not seen in the spectra of the 21 μm sources.

As originally proposed by Posch et al. (2004), FeO (iron monoxide or wüstite) nanoparticles seem to be a promising candidate carrier for the 21 μm feature for three reasons: (1) Fe is an abundant element; (2) FeO has a pronounced spectral feature around 21 μm ; and (3) except the 21 μm feature, FeO does not have any other notable spectral features. Posch et al. (2004) further argued that FeO nanoparticles could form and survive in the C-rich shells around the 21 μm sources (see §4.4.2 and Footnotes 7,8 of Zhang et al. 2009a; also see Begemann et al. 1995), provided that they are composed of $< 10^3$ atoms and have a size of $a \lesssim 1 \text{ nm}$. Iron oxides (particularly maghemite $\gamma\text{-Fe}_2\text{O}_3$ and magnetite Fe₃O₄) have also been suggested as a potential dust component in the interstellar medium (Jones 1990, Draine & Hensley 2013).

Posch et al. (2004) fitted the observed 21 μm emission feature with FeO of steady-state temperatures in thermal equilibrium with the stellar radiation field. However, with fewer than ~ 1000 atoms, FeO nanoparticles will be stochastically heated by single stellar photons as their heat capacities are smaller than or comparable to the energy of the stellar photons that heat them (see §5). Therefore, they will not attain an equilibrium temperature; instead, they will experience transient “temperature spikes” and undergo “temperature fluctuations” (see Draine & Li 2001). The stochastic heating of FeO nanoparticles by individual stellar photons will result in a distribution of temperatures and consequently, the emission spectra are expected to be broader than that from a single equilibrium temperature.

Zhang et al. (2009a) recognized the stochastic heating nature of FeO nanoparticles in PPNe. But they did not model the IR emission spectra of FeO nanoparticles; instead, they focused on the abundance constraint on Fe: they estimated the amount of Fe required to be locked up in FeO to account for the total emitted power of the 21 μm feature by assuming that FeO nanoparticles emit

at the peak temperature to which they are heated upon absorption of a typical stellar photon.

With an aim at examining the hypothesis of FeO nanoparticles as a carrier of the $21\ \mu\text{m}$ feature, we model the vibrational excitation and radiative relaxation of FeO nanoparticles in a proto-typical PPN – HD 56126 (see §4) – and then compare their model emission spectra with the observed $21\ \mu\text{m}$ feature. In §2 we discuss the optical properties of FeO. Their heat capacities are discussed in §3. In §4 we carry out calculations for the temperature probability distribution functions and the emergent IR emission spectra of FeO nanoparticles. §5 discusses the results and summarizes the major conclusions.

2. Optical Properties of FeO

To model the heating and cooling of FeO in PPNe, we need to calculate the absorption cross sections of FeO from the ultraviolet (UV) to the far-IR. This requires the knowledge of the optical properties of FeO. The optical properties of FeO vary with temperature T as the density of free charge carriers decreases with T . Since FeO nanoparticles will have a distribution of temperatures, we will consider their refractive indices at a range of temperatures.

Henning et al. (1995) measured the refractive indices of FeO at $T = 300\ \text{K}$ in the wavelength range of $\lambda = 0.2\ \mu\text{m}$ to $\lambda = 500\ \mu\text{m}$. Henning & Mutschke (1997) extended the same measurements to $T = 10, 100,$ and $200\ \text{K}$, but for a smaller wavelength range of $\lambda = 2\ \mu\text{m}$ to $\lambda = 500\ \mu\text{m}$.

For $T = 300\ \text{K}$, we adopt the refractive indices of FeO of Henning et al. (1995) from $\lambda = 0.2\ \mu\text{m}$ to $\lambda = 500\ \mu\text{m}$ (see Figure 1). For $T = 10, 100,$ and $200\ \text{K}$, the following synthetic approach is taken: for $\lambda = 2\ \mu\text{m}$ to $500\ \mu\text{m}$, we adopt the imaginary parts (m'') of the FeO refractive indices of Henning & Mutschke (1997) measured at $T = 10, 100,$ and $200\ \text{K}$;¹ for $\lambda < 2\ \mu\text{m}$ we adopt the imaginary parts m'' of FeO of Henning et al. (1995) measured at $T = 300\ \text{K}$, and then smoothly connect the m'' data at $\lambda < 2\ \mu\text{m}$ to that at $\lambda = 2\text{--}500\ \mu\text{m}$.² The Kramers-Kronig relation is then used to derive the real parts (m') of the indices of refraction of FeO at $T = 10, 100,$ and $200\ \text{K}$ from $\lambda = 0.2\ \mu\text{m}$ to $\lambda = 500\ \mu\text{m}$. Figure 1 shows the resulting refractive indices ($m = m' + i m''$) of FeO at $T = 10, 100, 200,$ and $300\ \text{K}$.

We note that, ideally, we should obtain the optical constants of FeO over a much wider wavelength range, from X-rays to millimeter wavelengths. However, the lack of experimental m'' data at $\lambda < 0.2\ \mu\text{m}$ and $\lambda > 500\ \mu\text{m}$ prevents us from achieving a complete set of (m', m'') data. Fortunately, for the present study this is not important: the stellar radiation of PPNe mostly peaks at the visible wavelength range, and FeO nanoparticles mostly emit their energy at $\lambda \sim 20\ \mu\text{m}$; there-

¹The m'' data of FeO of Henning & Mutschke (1997) for $T = 10, 100,$ and $200\ \text{K}$ are rather noisy at $10\ \mu\text{m} < \lambda < 15\ \mu\text{m}$ and at $\lambda > 70\ \mu\text{m}$. We have smoothed these data before we apply the Kramers-Kronig relation.

²The optical properties of FeO at $\lambda < 2\ \mu\text{m}$ are not sensitive to T as the free charge carriers (of which the densities are sensitive to T) mainly contribute to the far-IR continuum.

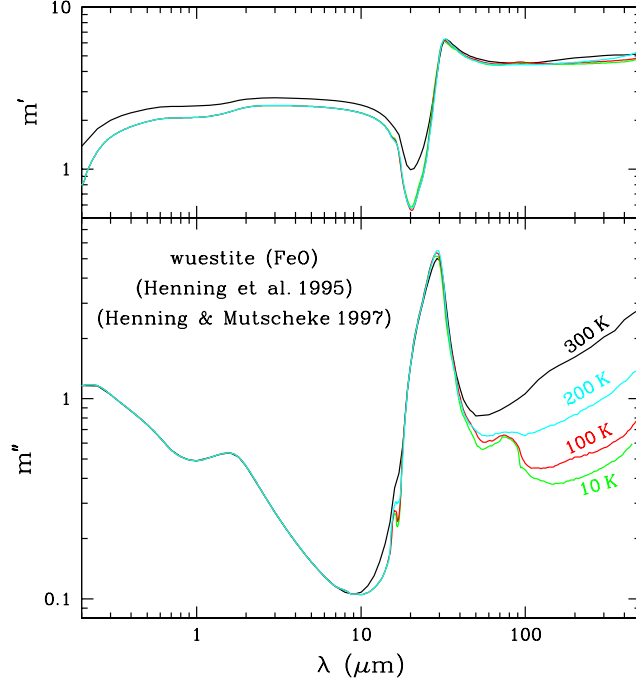


Fig. 1.— Optical constants m' (upper panel) and m'' (lower panel) of FeO at $T = 10$ K (green), 100 K (red), 200 K (cyan), and 300 K (black).

fore, the $m = m' + i m''$ data spanning the wavelength range of $0.2 \mu\text{m} < \lambda < 500 \mu\text{m}$ are sufficient for the present study.

3. Thermal Properties of FeO

FeO nanoparticles consist of several hundred atoms: with a mass density of $\rho \approx 5.7 \text{ g cm}^3$, a FeO grain of spherical radius of a has $N_{\text{atom}} \approx 400 (a/\text{nm})^3$ atoms. The vibrational degrees of freedom of FeO nano grains, $3(N_{\text{atom}} - 2)$, are so small that a single stellar photon of energy $h\nu$ is capable of appreciably raising their temperatures from T_i to T_f : $\int_{T_i}^{T_f} C(T) dT = h\nu$, where h is the Planck constant, ν is the photon frequency, and $C(T) \propto N_{\text{atom}}$ is the specific heat of FeO. At low temperatures (i.e., $T \ll \Theta_D$, where Θ_D is the Debye temperature), the specific heat is proportional to T^3 : $C(T) = (12\pi^4/5) N_{\text{atom}} k (T/\Theta_D)^3$, where k is the Boltzmann constant. As a prior, it is not clear if the condition of $T \ll \Theta_D$ will always be met for nano FeO in PPNe. Therefore, we shall not adopt this simple formula for $C(T)$; instead, we will adopt a three-dimensional Debye model with $\Theta_D \approx 430$ K which closely reproduces the experimental specific heat of FeO measured by Grønvold et al. (1993) and Stølen et al. (1996):

$$C(T) = 3(N_{\text{atom}} - 2)k f'_3(T/\Theta_D) \quad , \quad (1)$$

$$f_3(x) \equiv \int_0^1 \frac{3y^3 dy}{\exp(y/x) - 1} \quad , \quad f'_3(x) \equiv \frac{d}{dx} f_3(x) \quad . \quad (2)$$

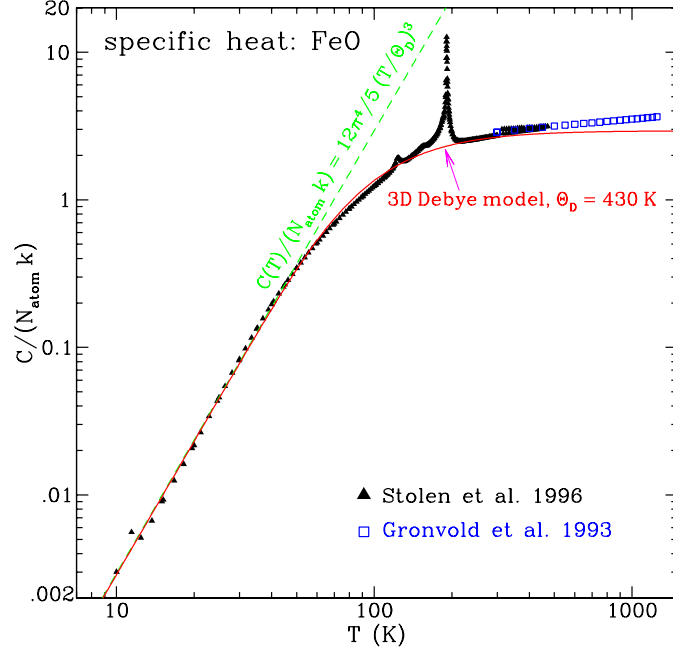


Fig. 2.— Comparison of the experimental specific heat of FeO measured by Grønvd et al. (1993; blue open squares) and Stølen et al. (1996; black filled triangles) and the specific heat given by the 3-dimensional Debye model with $\Theta_D = 430$ K (red solid line) and the low-temperature approximation of $C(T) \propto (T/430 \text{ K})^3$ (green dashed line). The peak at $T \approx 191$ K is due to the magnetic order-disorder transition.

In Figure 2 we show the experimental specific heat of FeO measured by Grønvd et al. (1993) for $298 \text{ K} < T < 1250 \text{ K}$ and by Stølen et al. (1996) for $10 \text{ K} < T < 450 \text{ K}$. Also shown are the 3-dimensional Debye model fit (with $\Theta_D = 430$ K) and the low-temperature approximation of $C(T) \propto (T/\Theta_D)^3$.

4. Results

Let $\kappa_{\text{abs}}(\lambda) = C_{\text{abs}}(a, \lambda)/m(a)$ be the mass absorption coefficient of FeO at wavelength λ , where $C_{\text{abs}}(a, \lambda)$ is the absorption cross section of FeO of size a at wavelength λ , and $m(a)$ is the mass of FeO of size a . For FeO nanoparticles in the IR, $\kappa_{\text{abs}}(\lambda)$ is independent of a since they are in the Rayleigh regime (i.e., $a \ll \lambda$). The IR emissivity per unit mass (in unit of $\text{erg s}^{-1} \text{ cm}^{-1} \text{ g}^{-1}$) from FeO nanoparticles of size a located at a distance of r from the illuminating star is

$$j_\lambda(r, a) = \kappa_{\text{abs}}(\lambda) \int_0^\infty dT \, 4\pi B_\lambda(T) \, dP(r, a, T)/dT \quad , \quad (3)$$

where $B_\lambda(T)$ is the Planck function of temperature T at wavelength λ , $dP(r, a, T)$ is the probability that the temperature of a FeO nanoparticle of size a at a distance of r from the illuminating star will be in $[T, T + dT]$. The total IR emissivity per unit mass from FeO nanoparticles of size a is obtained by integrating over the entire dust shell

$$j_\lambda^{\text{tot}}(a) = \int_{r_{\text{min}}}^{r_{\text{max}}} dr j_\lambda(r, a) 4\pi r^2 dn(r)/dr \quad , \quad (4)$$

r_{min} and r_{max} are respectively the inner and outer edge of the dust shell, and $dn(r)/dr$ is the FeO dust spatial distribution. The power output per unit mass in the $21\ \mu\text{m}$ band is calculated by integrating $\Delta j_\lambda^{\text{tot}}(a)$ over the entire band, where $\Delta j_\lambda^{\text{tot}}(a)$ is the continuum-subtracted $j_\lambda^{\text{tot}}(a)$

$$P_{21\mu\text{m}}(a) = \int_{21\mu\text{m band}} \Delta j_\lambda^{\text{tot}}(a) d\lambda \quad . \quad (5)$$

The FeO mass $M(\text{FeO})$ required to account for the observed $21\ \mu\text{m}$ emission is

$$M(\text{FeO}) = E_{21\mu\text{m}}^{\text{obs}}/P_{21\mu\text{m}}(a) \quad , \quad (6)$$

where $E_{21\mu\text{m}}^{\text{obs}}$ (in unit of erg s^{-1}) is the total power emitted from the $21\ \mu\text{m}$ feature. Let M_{H} be the total H mass in the shell. The Fe abundance (relative to H) required to be locked up in FeO is

$$[\text{Fe}/\text{H}]_{\text{FeO}} = M(\text{FeO})/[\mu_{\text{FeO}} M_{\text{H}}] \quad , \quad (7)$$

where $\mu_{\text{FeO}} = 72$ is the molecular weight of FeO.

We take HD 56126, a proto-typical $21\ \mu\text{m}$ source, as a test case. HD 56126 (\equiv IRAS07134+1005), a bright post-AGB star with a spectral type of F0-5I and a visual magnitude of ~ 8.3 , is one of the four $21\ \mu\text{m}$ sources originally discovered by Kwok et al. (1989). Mid-IR imaging of this object at $11.9\ \mu\text{m}$ shows that its circumstellar dust is confined to an area of $1.2''$ – $2.6''$ from the star (Hony et al. 2003). Detailed modeling of its dust IR spectral energy distribution suggested a $dn(r)/dr \sim 1/r$ dust spatial distribution at $1.2'' < r < 2.6''$. Following Hony et al. (2003), we will adopt a distance of $d \approx 2.4\ \text{kpc}$ to the star (and therefore $r_{\text{min}} \approx 4.3 \times 10^{16}\ \text{cm}$, $r_{\text{max}} \approx 9.3 \times 10^{16}\ \text{cm}$), a stellar radius of $r_\star \approx 49.2 r_\odot$ (r_\odot is the solar radius), a stellar luminosity of $L_\star \approx 6054 L_\odot$ (L_\odot is the solar luminosity), and approximate the HD 56126 stellar radiation by the Kurucz (1979) model atmospheric spectrum with $T_{\text{eff}} = 7250\ \text{K}$ and $\log g = 1.0$. These parameters determine the starlight intensity which vibrationally excites FeO nanoparticles.

We adopt the ‘‘thermal-discrete’’ method developed by Draine & Li (2001) to treat the stochastic heating of FeO nanoparticles. The necessity to model the stochastic excitation of FeO nanoparticles in the dust shell around HD 56126 will be justified in §5. For FeO dust of given size a at a given distance of r from the star, $P(r, a, T)$ – the temperature probability distribution function – is calculated from the ‘‘thermal-discrete’’ method. We first consider spherical dust and use Mie theory to calculate the absorption cross section $C_{\text{abs}}(a, \lambda)$ of FeO of radius a at wavelength λ . We adopt the refractive indices of FeO of $T = 100\ \text{K}$ (see Figure 1). As will be seen below, this is justified because for nano FeO the temperature probability distribution peaks around $\sim 100\ \text{K}$.

Figure 3 shows the temperature probability distribution functions $P(r, a, T)$ for spherical FeO of radius $a = 1$ nm at a distance of $1.20''$, $1.46''$, $1.77''$, $2.14''$, and $2.60''$ from the star. The $P(r, a, T)$ distribution functions are broad, confirming that nano FeO undergoes temperature excursions in PPNe [otherwise $P(r, a, T)$ should be strongly peaked and approximated by a delta function]. At a larger distance from the star, $P(r, a, T)$ becomes broader because of the reduced starlight intensity which leads to a smaller photon absorption rate and therefore enhances the single-photon heating effect. We also note that for $a \gtrsim 1$ nm $P(r, a, T)$ roughly peaks at $T \sim 100$ K (although the distribution function P is still appreciably broad for $a < 3$ nm), implying that the absorbed photon energy of FeO will be mostly radiated away at $T \sim 100$ K. This justifies the choice of the (m', m'') data of FeO of $T \sim 100$ K.

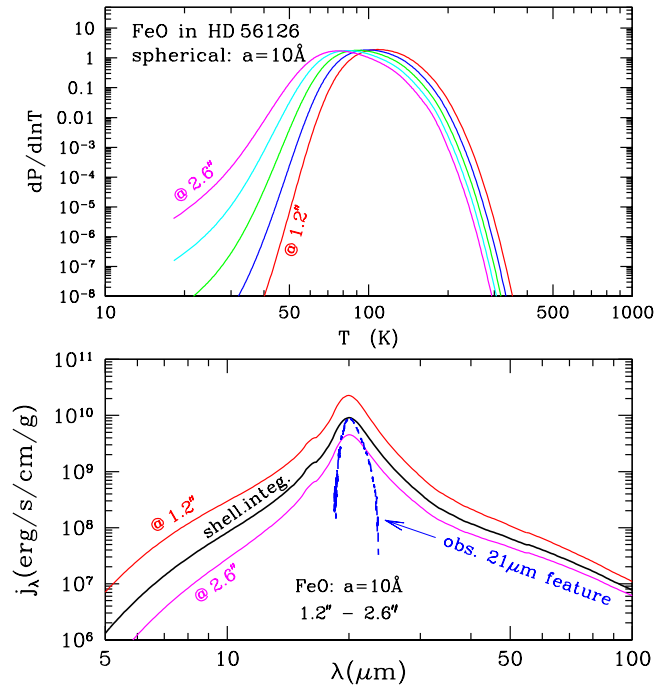


Fig. 3.— Upper panel: the temperature probability distribution functions of spherical FeO of radius $a = 1$ nm in HD 56126 at various distances (red: $1.20''$, blue: $1.46''$, green: $1.77''$, cyan: $2.14''$, and magenta: $2.60''$) from the star. Lower panel: the IR emissivity per unit mass of FeO of radius $a = 1$ nm at $1.20''$ (red) and $2.60''$ (magenta) from the star, and that integrated over the entire shell (thick black). Also shown is the observed $21 \mu\text{m}$ emission feature of HD 56126 (blue dashed; Volk et al. 1999) which is scaled to the shell-integrated model spectrum.

Figure 3 also shows the IR emissivity per unit mass $j_\lambda(r, a)$ of spherical FeO of radius $a = 1$ nm at $1.20''$ and $2.60''$, as well as that integrated over the entire shell $j_\lambda^{\text{tot}}(a)$.³ It is apparent that the model feature, with a FWHM of $\gamma_{21\mu\text{m}} \approx 3.7 \mu\text{m}$, is too broad to explain the $21 \mu\text{m}$ feature of HD 56126 which has a FWHM of $\sim 2.2 \mu\text{m}$ (see Footnote-1 of Zhang et al. 2009a). For illus-

³Following Hony et al. (2003), we take $dn(r)/dr \propto 1/r$.

tration, we compare in Figure 4 the model spectrum of FeO of $a = 10 \text{ \AA}$ with the $21 \mu\text{m}$ emission spectra observed in four C-rich PPNe (Volk et al. 1999): IRAS 04296 + 3429, IRAS 22272 + 5425, IRAS 23304 + 6147, and IRAS 07134 + 1005 (i.e., HD 56126), with each spectrum normalized to its peak value. Figure 4, in linear abscissa and ordinate, clearly shows that the FeO model results in too broad a $21 \mu\text{m}$ feature to explain the observed one, while observationally, the $21 \mu\text{m}$ feature in all sources has an (almost) identical intrinsic spectral profile (see Volk et al. 1999).

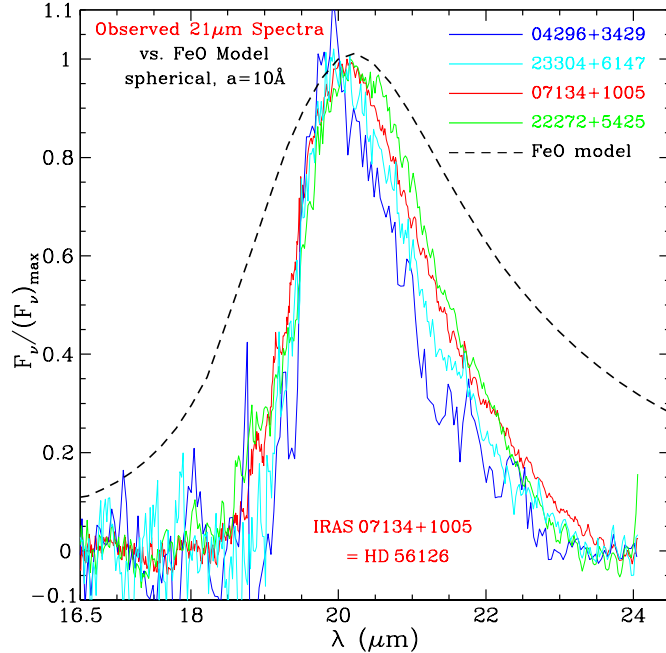


Fig. 4.— Comparison of the shell-integrated $21 \mu\text{m}$ emission feature calculated from spherical FeO of $a = 10 \text{ \AA}$ in the dust shell around HD 56126 (black dashed line; see the thick black line in Figure 3) with that observed in four C-rich PPNe (Volk et al. 1999): IRAS 04296 + 3429 (blue), IRAS 22272 + 5425 (green), IRAS 23304 + 6147 (cyan), and IRAS 07134 + 1005 (\equiv HD 56126; red). The $21 \mu\text{m}$ feature predicted from FeO is too broad to explain the observed feature.

With $E_{21\mu\text{m}}^{\text{obs}} \approx 1.0 \times 10^{36} \text{ erg s}^{-1}$ for the $21 \mu\text{m}$ emission feature of HD 56126 (Hony et al. 2003) and $M_{\text{H}} \approx 0.20 M_{\odot}$ for the circumstellar envelope of HD 56126 (Zhang et al. 2009b),⁴ we calculate a total FeO mass of $M(\text{FeO}) \approx 2.38 \times 10^{29} \text{ g}$ which is required to account for the $21 \mu\text{m}$ emission feature. The Fe abundance required to be locked up in FeO is $[\text{Fe}/\text{H}]_{\text{FeO}} \approx 8.31 \times 10^{-6}$, exceeding what is available in HD 56126 ($[\text{Fe}/\text{H}]_{\star} \approx 3.24 \times 10^{-6}$; van Winckel & Reyniers 2000) by a factor

⁴The mass of the circumstellar envelope of HD 56126 is not precisely known. Hony et al. (2003) derived a circumstellar envelope mass of $M_{\text{H}} \sim 0.16\text{--}0.44 M_{\odot}$, depending on the assumed gas-to-dust ratio ($\sim 220\text{--}600$). Meixner et al. (2004) derived a much smaller mass of $M_{\text{H}} \sim 0.059 M_{\odot}$ based on the CO J = 1–0 line emission images. Zhang et al. (2009b) derived $M_{\text{H}} \sim 0.20 M_{\odot}$, a value which is intermediate between the estimation of $M_{\text{H}} \sim 0.16\text{--}0.44 M_{\odot}$ of Hony et al. (2003). We therefore adopt $M_{\text{H}} \sim 0.20 M_{\odot}$.

of ~ 2.6 .⁵

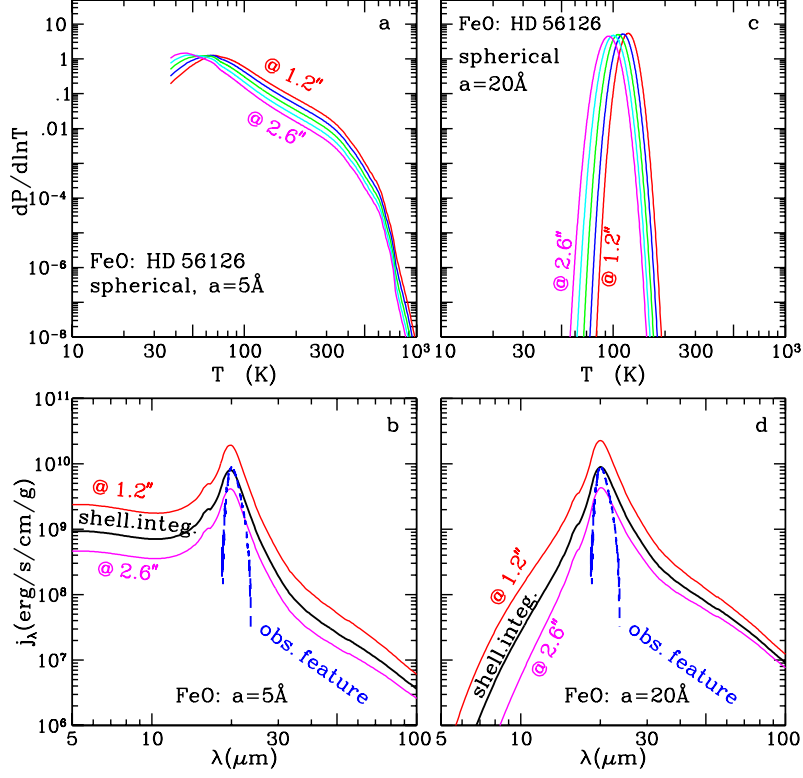


Fig. 5.— Same as Figure 3 but for FeO of $a = 5 \text{ \AA}$ (left panels: a, b) and $a = 2 \text{ nm}$ (right panels: c, d).

Similarly, we have calculated the $P(r, a, T)$ distribution functions and the IR emission spectra for FeO nanoparticles of $a = 5 \text{ \AA}$ and $a = 2 \text{ nm}$ (see Figure 5). Compared to that of FeO of $a = 1 \text{ nm}$, the $P(r, a, T)$ distribution function for $a = 5 \text{ \AA}$ is much broader and is appreciably large even at $T > 300 \text{ K}$. This is because for the $a = 5 \text{ \AA}$ FeO (with only ~ 50 atoms), its heat capacity is only 1/8 of that of the $a = 1 \text{ nm}$ FeO and therefore it can be heated to a much higher temperature by the same stellar photon. On the other hand, with a cross section only 1/4 of that of the $a = 1 \text{ nm}$ FeO, its photon absorption rate is also just 1/4 of that of the $a = 1 \text{ nm}$ FeO, and therefore, the single-photon heating effect becomes more pronounced for the $a = 5 \text{ \AA}$ FeO. In contrast, the $a = 2 \text{ nm}$ FeO, with a heat capacity eight times that of the $a = 1 \text{ nm}$ FeO, the $P(r, a, T)$ distribution function is more narrowly peaked at its “equilibrium” temperature of $T \approx 120 \text{ K}$ (see Figure 5), implying

⁵Zhang et al. (2009a) derived $[\text{Fe}/\text{H}]_{\text{FeO}} \approx 5.76 \times 10^{-7}$ by assuming FeO emits at the peak temperature which it reaches upon absorption of a typical stellar photon. They adopted a Debye temperature of $\Theta_{\text{D}} = 650 \text{ K}$ which is higher than $\Theta_{\text{D}} \approx 430 \text{ K}$ derived here by a factor of ~ 1.5 . For a given stellar photon, this would overestimate the FeO temperature by a factor of $\sim 1.5^{3/4} \approx 1.36$ and therefore underestimate the required FeO mass by a factor of $\sim 1.36^6 \approx 6.2$.

that the single-photon heating effect becomes less significant for larger FeO dust. The criterion for single-photon heating will be discussed in detail in §5.

The model 21 μm feature from the $a = 5 \text{ \AA}$ FeO, with a FWHM $\gamma_{21\mu\text{m}} \approx 3.6 \mu\text{m}$, is also too broad compared to that of the observed feature. To account for the 21 μm emission feature observed in HD 56126, the $a = 5 \text{ \AA}$ FeO requires $M(\text{FeO}) \approx 2.78 \times 10^{29} \text{ g}$ and $[\text{Fe}/\text{H}]_{\text{FeO}} \approx 9.70 \times 10^{-6}$. For the $a = 2 \text{ nm}$ FeO, the corresponding numbers are $\gamma_{21\mu\text{m}} \approx 3.7 \mu\text{m}$, $M(\text{FeO}) \approx 2.54 \times 10^{29} \text{ g}$, and $[\text{Fe}/\text{H}]_{\text{FeO}} \approx 8.87 \times 10^{-6}$.

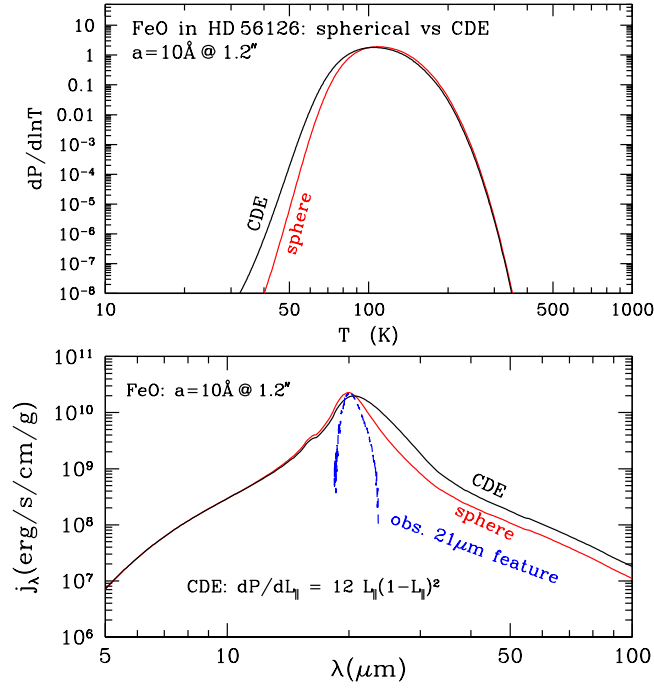


Fig. 6.— Upper panel: the temperature probability distribution functions of (1) spherical FeO (red) and (2) spheroidal FeO with a distribution of shapes (black) of radius $a = 1 \text{ nm}$ in HD 56126 at $1.20''$ from the star. Lower panel: the IR emissivity per unit mass of (1) spherical FeO (red) and (2) spheroidal FeO with a distribution of shapes (black) of radius $a = 1 \text{ nm}$ at $1.20''$ from the star. Also shown is the observed 21 μm emission feature of HD 56126 (blue dashed; Volk et al. 1999) which is scaled to that of spherical FeO. The 21 μm feature arising from the spherical $a = 1 \text{ nm}$ FeO (with a FWHM of $\gamma_{21\mu\text{m}} \approx 3.5 \mu\text{m}$) is much narrower than that of spheroidal FeO with a distribution of shapes (for which the FWHM is $\gamma_{21\mu\text{m}} \approx 5.6 \mu\text{m}$).

5. Discussion

We have seen in §4 that FeO nanoparticles emit strongly at 21 μm . However, the model 21 μm feature (with a FWHM of $\gamma_{21\mu\text{m}} \approx 3.6\text{--}3.7 \mu\text{m}$) is much broader than the observed feature (with a FWHM of $\sim 2.2 \mu\text{m}$). The Fe abundance required to be locked up in FeO ($[\text{Fe}/\text{H}]_{\text{FeO}}$) exceeds the available abundance $[\text{Fe}/\text{H}]_\star$ by a factor of $\sim 2.6\text{--}3$. These results are obtained for spherical grains.

For nonspherical grains, the model $21\ \mu\text{m}$ feature would be even broader. We have calculated the IR emission spectra for FeO nanoparticles with a distribution of spheroidal shapes with $dP/dL_{\parallel} = 12L_{\parallel}[1 - L_{\parallel}]^2$ (Ossenkopf et al. 1992) where $0 < L_{\parallel} < 1$ is the so-called “depolarization factor” parallel to the grain symmetry axis (for spheres $L_{\parallel}=1/3$); this shape distribution peaks at spheres and drops to zero for the extreme cases $L_{\parallel} \rightarrow 0$ (infinitely thin needles) or $L_{\parallel} \rightarrow 1$ (infinitely flattened pancake). As shown in Figure 6, the model $21\ \mu\text{m}$ emission feature arising from FeO nanoparticles with such a distribution of spheroidal shapes is much broader than that of spherical FeO.

In calculating the absorption cross sections of FeO, we use the optical constants of $T = 100\ \text{K}$. As shown in Figure 9 of Posch et al. (2004), the absorption profile of the $21\ \mu\text{m}$ band broadens if one adopts the optical constants of $T = 200, 300\ \text{K}$, while essentially it remains unchanged from $T = 100\ \text{K}$ to $T = 10\ \text{K}$. Although small, $P(r, a, T)$ is positive at $T > 200\ \text{K}$ for $a \lesssim 1\ \text{nm}$ (see Figures 3,5). Therefore, if we adopt the (m', m'') data of $T \gtrsim 200\ \text{K}$ for FeO warmer than $200\ \text{K}$, we would expect a broader $21\ \mu\text{m}$ emission feature. Nevertheless, we note that the $21\ \mu\text{m}$ feature of nano FeO calculated in this work is based on the dielectric functions of bulk FeO material (see §2). It is not clear how the dielectric functions near the $21\ \mu\text{m}$ resonance wavelength range will be affected when FeO becomes nano-sized.

For a small *metallic* grain, the imaginary part of its dielectric function is expected to be larger compared to that of its bulk counterpart, as a consequence of the so-called *electron mean free path limitation* effect (see §6 in Li 2004). For FeO which is a *semiconductor* (Seagle et al. 2009, Schrettle et al. 2012), the number density of free charge carriers is lower than that of metals by several orders of magnitude (see Henning & Mutschke 1997). Therefore, the small size effect on the dielectric function caused by the limitation of the electron mean free path is expected to be less significant for FeO than for metals.

We also note that the thermal properties of nano FeO may differ from that of bulk material (see §3). The specific heats of some small metal particles are reported to be strongly enhanced over their bulk values (see §6 in Li 2004). It is not clear how the Debye temperature Θ_{D} of nano FeO would compare to that of bulk FeO. If nano FeO is like palladium (with $\Theta_{\text{D}} \approx 273\ \text{K}$ for bulk palladium and $\Theta_{\text{D}} \approx 175\ \text{K}$ for nano palladium of $a = 1.5\ \text{nm}$), the stochastic heating effect will be less substantial.⁶ But we also note that the specific heats of nano silicon crystals and nanocrystalline diamonds do not differ much from their bulk values (see §6 in Li 2004).

Finally, we note that ideally, we should have justified why, in the first place, it is necessary to consider the stochastic heating of nano FeO. It is now well recognized that a grain undergoes stochastic heating by single stellar photons if (i) its heat content is smaller than or comparable

⁶With a smaller Debye temperature Θ_{D} , the specific heat $C(T) \propto (T/\Theta_{\text{D}})^3$ increases. Therefore, upon absorption of a photon of energy $h\nu$, the temperature rise ΔT (from the initial temperature T_i to the final temperature T_f) will be less: $\Delta T = T_f - T_i, \int_{T_i}^{T_f} C(T)dT = h\nu$.

to the energy of a single stellar photon (Greenberg 1968), and (ii) the photon absorption rate is smaller than the radiative cooling rate (Draine & Li 2001).

The photon absorption time scale — the mean time τ_{abs} between photon absorptions — for a nano FeO of size a is given by

$$\tau_{\text{abs}}^{-1} \equiv \int_0^\infty C_{\text{abs}}(a, \lambda) \frac{cu_\lambda}{hc/\lambda} d\lambda \quad , \quad (8)$$

where c is the speed of light, h is the Planck constant, and u_λ is the starlight energy density. The mean photon energy $\langle h\nu \rangle_{\text{abs}}$ absorbed by the FeO dust of size a is

$$\langle h\nu \rangle_{\text{abs}} \equiv \tau_{\text{abs}} \int_0^\infty C_{\text{abs}}(a, \lambda) cu_\lambda d\lambda \quad . \quad (9)$$

The radiative cooling time for a FeO grain of size a containing a vibrational energy of $\langle h\nu \rangle_{\text{abs}}$ is

$$\tau_{\text{cooling}} \approx \frac{\langle h\nu \rangle_{\text{abs}}}{\int_{\lambda_{\text{min}}}^\infty C_{\text{abs}}(a, \lambda) 4\pi B_\lambda(T_p) d\lambda} \quad , \quad (10)$$

where $\lambda_{\text{min}} \equiv hc/\langle h\nu \rangle_{\text{abs}}$ and T_p is determined by its heat content $E(T_p) = \int_0^{T_p} C(T) dT = \langle h\nu \rangle_{\text{abs}}$.

For nano FeO of $a < 30$ nm in the dust shell around HD 56126, the mean absorbed photon energy is $\langle h\nu \rangle_{\text{abs}} \approx 4.45$ eV, independent of dust size a . This is because in the UV/visible wavelength range nano FeO is in the Rayleigh regime and its absorption properties are independent of size a . In Figure 7a we show τ_{abs} and τ_{cooling} of FeO dust in the HD 56126 dust shell, at a distance of $r = 1.77''$ from the central star which is intermediate between the inner boundary and the outer boundary of the shell. It is apparent that $\tau_{\text{abs}} \propto a^{-2}$ rapidly decreases with a , while τ_{cooling} increases with a . It is clear that FeO dust of $a < 1.2$ nm, with $\tau_{\text{abs}} > \tau_{\text{cooling}}$, will be subject to substantial temporal fluctuations in temperature. For FeO dust of $a \gtrsim 5$ nm, with $\tau_{\text{abs}} \ll \tau_{\text{cooling}}$, will attain an equilibrium temperature.

In Figure 7b we compare the mean absorbed photon energy $\langle h\nu \rangle_{\text{abs}}$ with the heat content $E(T_{\text{ss}}) = \int_0^{T_{\text{ss}}} C(T) dT$ at $T_{\text{ss}} = 106$ K, the “equilibrium” or “steady-state” temperature which would be attained by FeO dust of $a \gtrsim 5$ nm at $r = 1.77''$. Again, it is seen that for FeO dust of a couple of nanometers in size, its heat content is comparable or smaller than the energy of a single stellar photon and its temperature will be appreciably raised upon absorption of an individual photon, while for FeO dust of $a \gtrsim 5$ nm, its heat content is much larger than the photon energy and therefore the absorption of a single photon will not change its temperature. This also justifies the necessity to consider the stochastic heating of nano FeO of $a < 5$ nm.

In Figure 7c we show the temperature probability distribution functions $dP/d\ln T$ for nano FeO of $a = 1.25, 2.5, 5, 10$ nm at $r = 1.77''$. These results confirm the conclusions drawn from the general considerations discussed in Figure 7a,b: for FeO dust of $a \gtrsim 5$ nm, with $\tau_{\text{abs}} \ll \tau_{\text{cooling}}$ and $E(T_{\text{ss}}) \gg \langle h\nu \rangle_{\text{abs}}$ at $T_{\text{ss}} \approx 106$ K, the temperature distribution function $dP/d\ln T$ is like a delta function, implying that it will attain an equilibrium temperature of $T_{\text{ss}} \approx 106$ K. According to Posch

et al. (2004), the size of the FeO dust which could form and survive in the C-rich shells around the $21\ \mu\text{m}$ sources should not exceed $\sim 1\ \text{nm}$. FeO dust this small will have $\tau_{\text{abs}} > \tau_{\text{cooling}}$ (see Figure 7a), and $E(T) < \langle h\nu \rangle_{\text{abs}}$ at $T_{\text{ss}} \approx 106\ \text{K}$ (see Figure 7b), and therefore will be stochastically heated by single stellar photons.

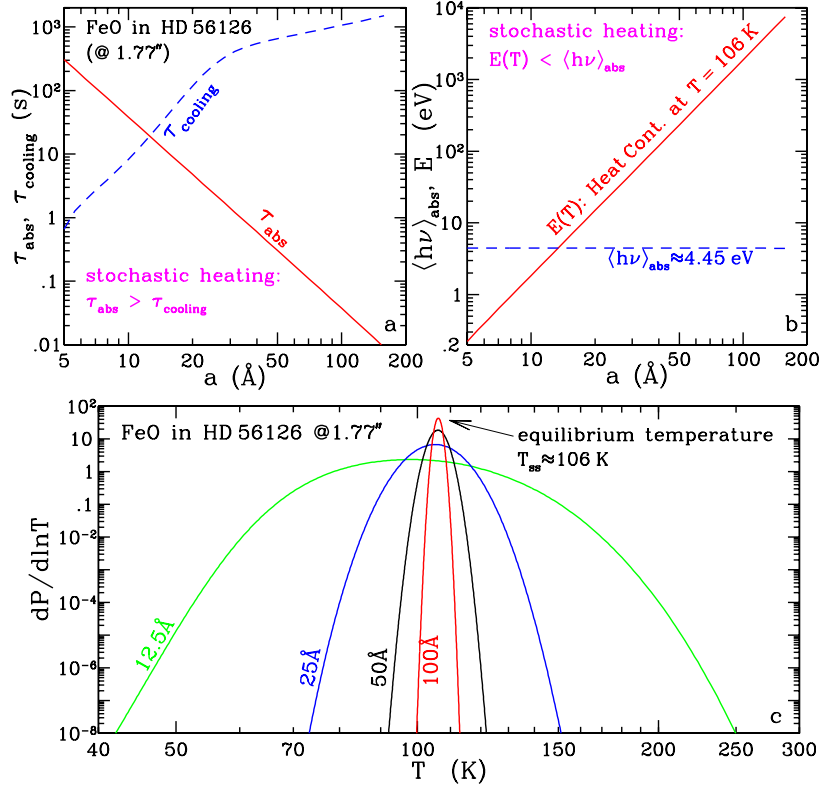


Fig. 7.— Upper left panel (a): Comparison of the radiative cooling time scale τ_{cooling} for FeO dust containing a vibrational energy of $\langle h\nu \rangle_{\text{abs}}$ with the photon absorption time scale τ_{abs} for FeO dust at $r = 1.77''$ in HD 56126. Upper right panel (b): Comparison of the mean absorbed photon energy $\langle h\nu \rangle_{\text{abs}} \approx 4.45\ \text{eV}$ with the heat content $E(T_{\text{ss}}) = \int_0^{T_{\text{ss}}} C(T) dT$ at $T_{\text{ss}} = 106\ \text{K}$, the “equilibrium” temperature which would be attained by FeO dust of $a \gtrsim 5\ \text{nm}$ at $r = 1.77''$ in HD 56126. Bottom panel (c): The temperature probability distribution functions of FeO dust at $r = 1.77''$ in HD 56126.

To summarize, we have examined the hypothesis of FeO nanoparticles as a carrier of the mysterious $21\ \mu\text{m}$ emission feature seen in C-rich PPNe. The temperature probability distribution functions and the resulting IR emission spectra have been calculated for these stochastically-heated nano-sized grains. We find that they emit too broad a $21\ \mu\text{m}$ feature to explain the observed one and the Fe abundance required to be locked up in FeO exceeds what is available. This, combined with the special conditions required for the formation of FeO nanoparticles in C-rich environments (see §3.3 of Posch et al. 2004, Duley 1980), leads us to conclude that probably FeO nanoparticles are not responsible for the $21\ \mu\text{m}$ feature.

We thank J. Gao and K. Zhang for their kind help in preparing for this manuscript. We thank K. Volk who kindly provided us the 21 μm emission spectra of the four PPNe shown in Figure 4. We thank S. Hony, A.P. Jones, C. Koike, P. Miceli, and the anonymous referee for helpful suggestions. We are supported in part by NSF AST-1109039, NNX13AE63G, NSFC 11173007, NSFC 11173019, NSFC 11273022, and the University of Missouri Research Board.

REFERENCES

- Begemann, B., Henning, Th., Mutschke, H., & Dorschner, J. 1995, *Planet. Space Sci.*, 43, 1257
- Cerrigone, L., Hora, J. L., Umana, G., Trigilio, C., Hart, A., & Fazio, G. 2011, *ApJ*, 738, 121
- Draine, B. T., & Li, A. 2001, *ApJ*, 551, 807
- Draine, B. T., & Hensley, B. 2013, *ApJ*, 765, 159
- Duley, W. W. 1980, *ApJ*, 240, 950
- Greenberg, J.M. 1968, in *Stars and Stellar Systems*, Vol. VII, ed. B.M. Middlehurst, & L.H. Aller, (Chicago: Univ. of Chicago Press), 221
- Grønvold, F., Stølen, S., Tolmach, P., & Westrum, E.F. 1993, *J. Chem. Thermodynamics*, 25, 1089
- Henning, Th., Begemann, B., Mutschke, H., & Dorschner, J. 1995, *A&AS*, 112, 143
- Henning, Th., & Mutschke, H. 1997, *A&A*, 327, 743
- Hony, S., Tielens, A.G.G.M., Waters, L.B.F.M., & de Koter, A. 2003, *A&A*, 402, 228
- Jiang, B.W., Zhang, K., & Li, A. 2010, *Earth, Planets, & Space*, 62, 105
- Jones, A.P. 1990, *MNRAS*, 245, 331
- Kurucz, R.L. 1979, *ApJS*, 40, 1
- Kwok, S., Volk, K., & Hrivnak, B.J. 1989, *ApJ*, 345, L51
- Li, A. 2004, *Astrophysics of Dust* (ASP Conf. Ser. 309), ed. A.N. Witt, G.C. Clayton, & B.T. Draine (San Francisco, CA: ASP), 417
- Ossenkopf, V., Henning, Th., & Mathis, J.S. 1992, *A&A*, 261, 567
- Posch, Th., Mutschke, H., & Andersen, A. 2004, *ApJ*, 616, 1167
- Schrettle, F., Kant, C., Lunkenheimer, P., Mayr, F., Deisenhofer, J., & Loidl, A. 2012, *Eur. Phys. J. B*, 85, 164

- Seagle, C. T., Zhang, W., Heinz, D. L., & Liu, Z. 2009, *Phys. Rev. B*, 79, 014104
- Stølen, S., Glöckner, R., Grønvold, F., Atake, T., & Izumisawa, S. 1996, *Am. Mineral.*, 81, 973
- van Winckel, H., & Reyniers, M. 2000, *A&A*, 354, 135
- Volk, K., Kwok, S., & Hrivnak, B.J. 1999, *ApJ*, 516, L99
- Volk, K., Hrivnak, B.J., Matsuura, M., et al. 2011, *ApJ*, 735, 127
- Zhang, K., Jiang, B. W., & Li, A. 2009a, *MNRAS*, 396, 1247
- Zhang, K., Jiang, B. W., & Li, A. 2009b, *ApJ*, 702, 680